Research Inventy: International Journal of Engineering And Science
Vol.13, Issue 10 (October 2023), PP 14-21
Issn (e): 2278-4721, Issn (p):2319-6483, www.researchinventy.com

Analysis of the impact of PMMA on the formation and variations of modes in the visible frequency domain using PIMI

NABIN TIMALSINA[1], ABBAS NASIR[1], ALBERT KABBAH[2], LIU XUEFUNG[1] AND XIONG JICHUAN[1*]

[1] *School of Electronics and Optical Engineering, Nanjing University of Science and Technology,210094, PR-China*

[2] *Nanjing University of Aeronautics and Astronautics,210016, PR-China*

**jichuan.xiong@njust.edu.cn*

Abstract: *This paper presents a simulation-based finite-difference time-domain method supported by the experiment for a metal-dielectric structure consisting of gold and PMMA discs stacked on top of one another on a glass substrate to analyze multiple resonant modes induced on the built-in structure. We found that altering the thickness and radius of the topped-up PMMA makes it possible to control the excited modes at corresponding extinction spectrum peak locations. Our conclusion is entirely confirmed by simulation and experiment that uses the PIMI methods algorithm, which creates images of field distribution with adequate information regarding Sinδ, ϕ, and I-dp.*

Keywords: *Hybrid metal-dielectric structure, Excited modes, Finite -difference time -domain method, PIMI.*

Date of Submission: 02-10-2023 Date of acceptance: 12-10-2023

I. Introduction

Plasmonic nanostructures exhibit strong electric field enhancement by the resonant oscillation of free electrons. Plasmonic nanostructures comprise coherent oscillations of free electrons that can be induced in metallic nanoparticles by the incoming light, a phenomenon called Localized surface plasmon resonances, or LSPRs. It is known that the restoring force is applied to the oscillating electrons, strengthening the electric field close to the particle surface [1, 3]. A metal nanostructure's plasmon resonances (modes) can be defined as dipole, quadrupole, or high-order modes depending on the surface charge distribution induced by the incident light. The plasmonic mode is primarily sustained by the nanostructures mounted on surfaces with higher refractive index (RI) values than air, with a near-field distribution restricted to the substrate [11]. These modes are sensitive to nanostructure size, shape, morphology, the chosen metal material, and the RI of the surrounding medium [4, 5]. A plasmonic nano-object may exhibit high-order resonances such as the quadrupole, hexapole, octupole, and dipolar mode excitation [6, 9].

Similarly, the plasmonic modes can be categorized into bright and dark categories based on their optical properties [10]. In some instances, the redistribution of the field also coincides with the spectral development of a new mode with the opposite field distribution and highest field strength at the top of the nanostructure [12, 14]. Symmetry breaking caused by the addition of substrate results in the coupling of dark and bright modes. This can be accomplished by depositing a nanoparticle or constructing a nanostructure using deposition methods onto a dielectric substrate [15, 17]. The "image" of dipolar plasmon results from the nanoparticle placed on a dielectric substrate with a significant quadrupolar field component across the nanoparticle. This introduces a coupling between its dipolar and quadrupolar plasmons, leading to hybridized plasmon superpositions of dipolar and quadrupolar modes. Two bright modes for a single silver nanocube near the substrate were demonstrated experimentally and numerically by Sherry et al. [18].

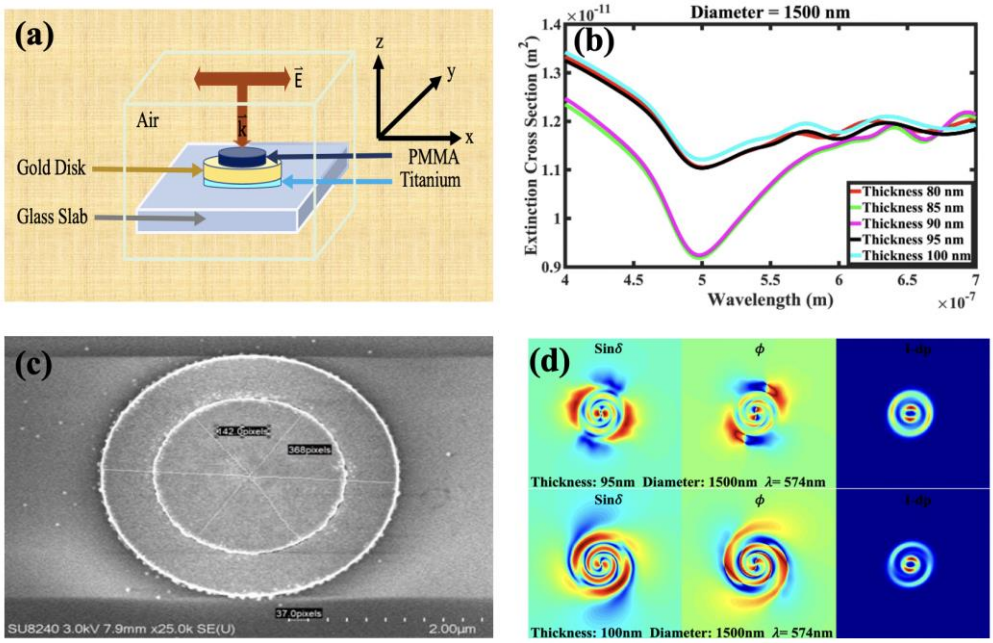

Fig. 1. Principle Diagram for the built-in nanostructure. Fig. 1(a) shows the front view. Fig. 1(b) Presents the extinction cross-section curve for the PMMA disk of diameter 1500 nm and various thicknesses. Fig. 1(c) presents the SEM image of the PMMA topped up on a gold disk placed over a glass substrate. Fig.1(d) presents the PIMI parameters for the two different thicknesses at the same wavelength.

Based on the hybridization theory, Zhang et al. suggested a model account for forming these modes [19]. The Authors [20] also propose an experimental and numerical study of the hybridized plasmonic modes of silver nanocylinders and de-hybridization after covering the silver layer with a polymer that induces uncoupled multipolar resonance. We here use a PMMA disk topped on gold, a diameter of 3000 nm and a thickness of 70 nm, placed on the glass substrate. Using polarization parametric indirect microscopic imaging parameters (PIMI) [24]., we present a thorough study of the multiple excited modes. We further elucidate the impact of the geometry on the multiple-mode excitation. This work enables the precise description of the excited mode corresponding to the ideal wavelength using pictures of Sinδ, ϕ, and I-dp of distributed field.

1. Methods for metal-dielectric structure, gold disc, and a resist material (PMMA) disk stacked one on top of another, topped on a silica substrate

Numerical modeling analyzes the field distribution patterns and explicit extinction cross sections of a metallic gold disk on the quartz glass. The parameter we used here for simulation for a metallic gold disk on the quartz glass was the same as those used for a topped-up resist disk on a metallic gold disk patterned on quartz glass. We employ Lumerical simulation FDTD tools [21] to simulate this scenario. A single sample, whose PMMA thickness and diameter are 100 nm and 1500 nm, respectively, was used for the experiment. Figure 1(a) illustrates schematic geometrical structures of a plane wave incident light along the negative z-axis perpendicular to the cylindrical disc of resist material on a cylindrical layer of metallic gold over the quartz glass. The following simulation uses a PML (Perfectly matched layer-absorbing border) as a boundary condition and defaults mesh sizes. The computation is $10 \times 10 \times 1.5\ \mu m^3$. The Lorenz-Drude model [22] was used to describe the dielectric behavior of a micro gold disc. The surrounding medium's refractive index was fixed at 1.0 for air, the PMMA's refractive index was assumed to be 1.5, and the glass refractive index was determined from Palik [23]. The hybrid metal-dielectric structure's field intensity distribution is set up using simulations and experiments based on PIMI [24].

Figure 1(a) shows the arrangement of an Au disc with a constant radius of 1500 nm and thickness of 70 nm and a PMMA disc with a changeable diameter from 500 nm to 3000 nm at a difference of 500 nm for each thickness that ranges from 80 nm to 100 nm at a difference of 5 nm.

II. Result and Analysis:

A. A metallic gold disk on a glass substrate without topping PMMA resist

This study focuses on a metallic gold disc that produces a non-uniform electric field due to the incident field when its diameters exceed one-fourth of the illumination wavelength. This causes a phase or amplitude change, depending on the distribution of the surface charge, which in turn excites several resonance modes. Fig. 2(g) (red curve) shows the extinction cross-section curves that most likely result from surface plasmons generated in a micro gold disc, which have significantly dipped at 487 nm, which is sensitive to the size of the gold disc and tiny peaks at 580 nm and 667 nm, respectively. Depending on the thickness of the gold disc, a higher-order mode, like quadrupolar and hexapolar, are assumed to have generated the two smaller peaks at 574 nm and 667 nm. The tiny dip between these modes indicates the interference between them.

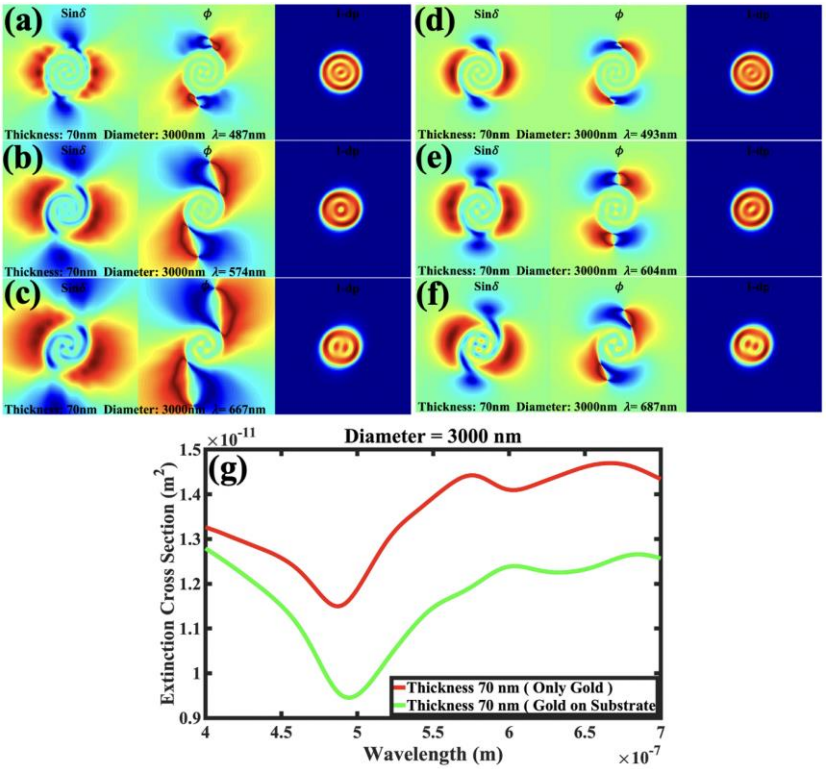

Fig. 2 shows PIMI parameters for a gold disk on a glass substrate and the Cross-section spectrum. Fig. 2(a-c) shows PIMI parameters for the field distribution for a single gold disk at a wavelength of 487 nm, 574 nm, and 667 nm, respectively. Fig. 2(d-f). shows PIMI parameters for the field distribution for a gold disk on a glass substrate at a wavelength of 493 nm, 604 nm, and 687 nm.

Fig. 2(g) (green curve) shows the extinction cross-section of a gold disc with a fixed diameter of 3000 nm and thickness of 70 nm placed on a glass substrate. The glass has a higher refractive index than air, creating a different dielectric environment for the gold disc, dramatically affecting the extinction cross-section curve. For each resonance frequency, the values of the cross-section are typically decreased when the gold disc is in contact with the substrate. This is because there is a possibility that interaction between the plasmon modes in the disc and the modes supported by the substrate will lead to energy dissipation and dampening of the plasmon resonances, which leads to the curve redshifted along with the decrease in values of Extinction Cross section. The plasmon modes have changed due to the coupling between the gold disc and the mode supported by the glass substrate, which is a typical side effect of plasmon hybridization. The surface plasmon's electromagnetic fields may interact with the glass substrate when the gold disc is close to it, changing the resonance characteristics of the plasmons. Therefore, PIMI parameters of the distributed field for different wavelengths observed in the peaks and valleys are created by using PIMI imaging techniques to scattered fields that the monitor with its XY plane records oriented at a few micrometers distant from the top surface of the gold disc. Fig. 2(a) shows PIMI parameters for the field produced at the wavelength of 487 nm, which we can observe as the single gold. Similarly, Fig. 2(b, c) display the PIMI parameters of the field at a wavelength where the two peak modes emerged at 574 nm and 667 nm, the same as gold on a glass substrate.

B. A topped-up resist disk on a metallic gold disk patterned on quartz glass

First, the PMMA disc we used for my first experiment had a 1500 nm diameter and a 100 nm thickness. When I compared the experimental result to the simulation result for the same sample, I found that the findings from the simulation and the experiment were quite close. Based on this information, we continued to perform simulations with various diameter and thickness settings, considering that the results would also apply to additional samples with varying diameters and thicknesses.

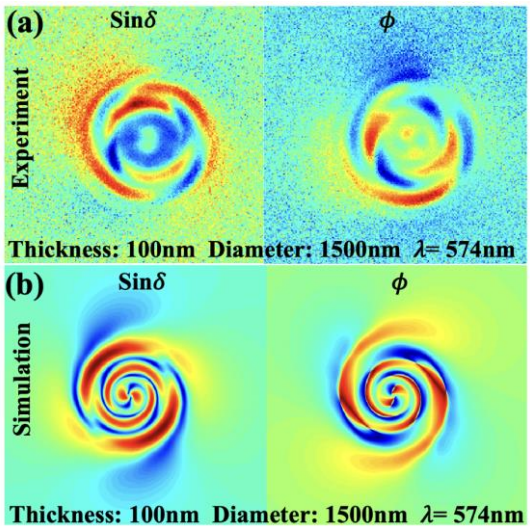

Fig. 3 Shows the PIMI parameters of a PMMA disk of diameter 1500 nm and variable thickness topped up on a gold disk on a glass substrate. Fig. 3(a, b). shows PIMI characteristics for the field distribution at a wavelength of 574 nm for 100 nm thickness were acquired experimentally and by simulation, respectively.

We investigated a PMMA disc with changeable diameter and thickness topped on a gold disc with a 3000 nm diameter and a 70 nm thickness. The effective refractive index of the system can change when the PMMA disc is placed on top of the gold disc, which further alters the plasmon's resonance frequency and the extinction spectrum and widening of the dip. Phase variation due to changes in effective refractive index and a retardation effect by having a significant amount of thickness and diameter of PMMA allowed us to observe multiple excitation modes. These effects, which are not a function of hybridization, are more apparent due to retardation, which alters the dip of the extinction cross-section curve. In addition, the fact that the interaction between the incident light and the plasmonic modes of the gold disc is sensitive to the refractive index contrast at the interface helps to explain the shift towards longer wavelengths. PMMA disc of all diameters, for the thickness of 80 nm, 95 nm, and 100 nm, if we compare the extinction cross-section curve with the one of gold on a glass substrate without topped-up PMMA, the primary dip widens as the diameter increases from 500 nm to 3000 nm. Also, we can see that the curve has been shifted vertically upward if we examine the overall curve for Fig. 4 and 7. This widening can be observed for 85 and 90 nm after the diameter exceeds 2000 nm. The vertical shift is not substantial for 85 nm and 90 nm thicknesses. Although the change is relatively small, the curve moves towards longer wavelengths as its diameter increases.

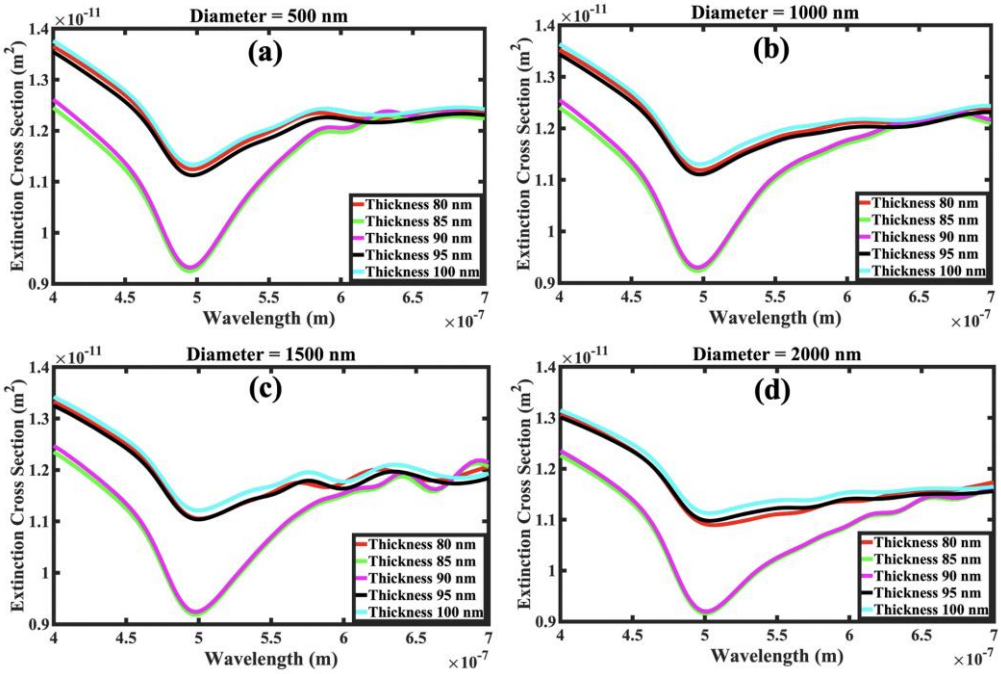

Fig. 4 Shows the cross-section spectrum for different diameters and thicknesses of PMMA. Fig. 4(a-c). Cross-section spectrum for the diameter of 500 nm, 1000 nm, 1500 nm, and 2000 nm with thicknesses of 80 nm, 85 nm, 90 nm, and 100 nm, respectively, for PMMA.

When the PMMA resists, thickness is changed by 5 nm from 80 nm to 100 nm while maintaining a diameter of 500 nm. In contrast to three excited modes at 85 and 90 nm, we observe two excited modes at 80 nm, 95 nm, and 100 nm. Compared to the curve that appears when only gold is topped on a glass substrate section, for the thickness of 80 nm, 95 nm, and 100 nm, the total curve moves vertically upward with an increased value of extinction cross-section. The overall intensity of the scattering at the thicknesses of 80 nm, 95 nm, and 100 nm is increasing, as indicated by the vertical shift and wider dip in the extinction cross-section curve. However, no noticeable shift towards the longer wavelength is visible. These thicknesses also share a similar number of higher-order modes, but these modes are noticeably wider than the ones we saw when there was a gold disk on the glass substrate.

Additionally, there is no vertical shift for 85nm and 90 nm thicknesses. The curve for a PMMA resist with a diameter of 1000 nm, and various thicknesses is shown in Fig. 4(b). As the disc diameter is increased to 1000 nm, we can see similar dips but slightly widened for the 80 nm, 95 nm, and 100 nm thickness. From the observation, for all the thickness, while observing extinction cross-section curve shows the presence of only primary dip, whereas higher order modes are absent. Possibly the destructive interference between higher-order modes cancels each other. Once again, as the diameter reaches 1500 nm, the extinction curve radically changes shape and develops a series of peaks, as shown in Fig. 4(c). Compared to the large observed dip in the 85 and 90 nm thickness curves, the dip observed for the thickness of 80nm, 95nm, and 100 nm diameter widens out. Two excited higher orders modes can be observed for all the thicknesses. Overall, the curves for 85 nm and 90nm seem to move vertically down infinitesimally, while for 80 nm,95 nm, and 100 nm, the curve seems to be fixed at the position without a further shift to the longer wavelength in comparison with the curves of a diameter of 1000 nm.

On the other hand, it's important to note that the PIMI image for one of the two higher-order modes produced when the thickness was 80 and 85 nm seems to be the same for different thicknesses at different wavelengths. The PIMI photos reveal that the first mode, stimulated at a wavelength of 641 for a thickness of 85 nm and depicted by the PIMI parameters in Figure 5, is likewise the second mode, excited with an 80 nm thickness at 624 nm. Further inferences may be drawn from Figures 5 and 4 that the wavelength at which the excited mode shows was redshifted when the thickness was increased from 80nm to 85nm.

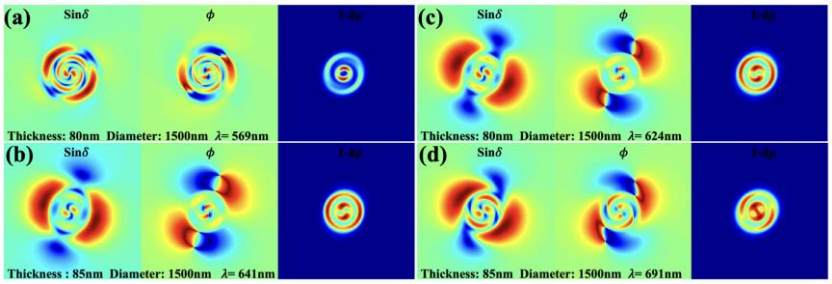

Fig. 5 Shows the PIMI parameters of a PMMA disk of diameter 1500 nm and variable thickness topped up on a gold disk on a glass substrate. Fig. 5(a, b) and Fig. 5(c, d) presents PIMI parameters for the field distribution at a wavelength of 569 nm, 641nm, and 624 nm, 691 nm for 80 and 85 nm thickness, respectively.

At 574 nm and 634 nm wavelengths, two higher-order modes are excited as the thickness approaches 95 nm. Similarly, two higher-order modes are also present at a thickness of 100 nm. The first mode was excited at the same wavelength of 574 nm for both 95 and 100 nm thicknesses. This indicates that changing the thickness at a fixed wavelength can modify the mode shape, as illustrated in Fig 6.

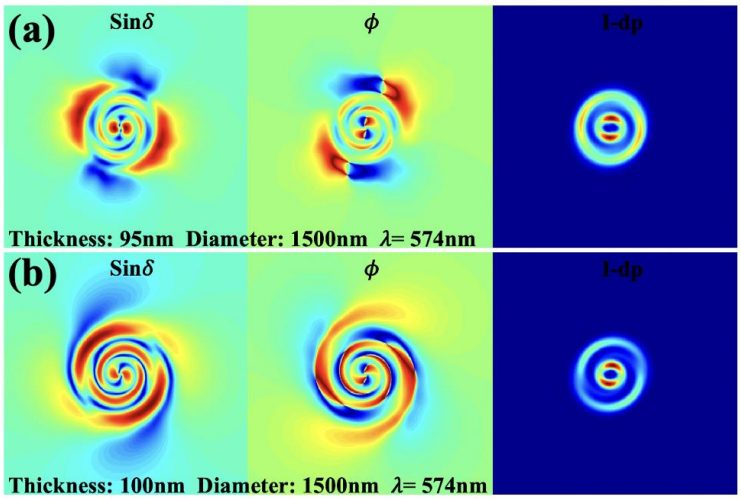

Fig. 6 Shows the PIMI parameters of a PMMA disk of diameter 1500 nm and variable thickness topped up on a gold disk on a glass substrate. Fig. 6(a, b). shows PIMI parameters for the field distribution at a wavelength of 574 nm for 95 nm and 100 nm thickness.

No higher-order modes are visible at all thicknesses when the diameter reaches 2000 nm, as shown in Fig. 4(d). The reason could be similar when the diameter was 1000 nm. Overall, the dip that occurred previously for the thickness of 80 nm, 95 nm, and 100 nm was completely spread out and flatted. Further, there is very little shift to the longer wavelength. The overall curves are significantly flat at a diameter of 2000 nm, but it becomes substantially flatter at 2500 nm, as shown in Fig. 7(a). For this diameter, the thicknesses of 80 nm, 95 nm, and 100 nm each show three higher modes. However, the thicknesses of 90 nm and 85 nm are seen to have two higher-order modes. Higher order modes look very strong from the thickness of 80 nm,95 nm, and 100 nm, and the dipolar mode has disappeared.

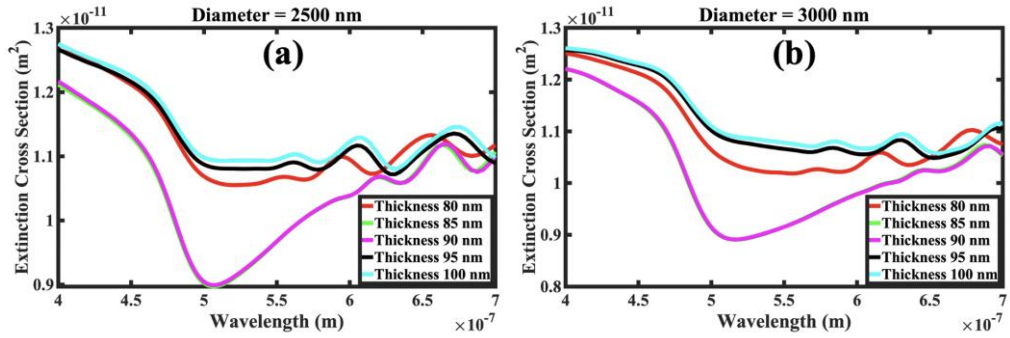

Fig. 7 shows the spectrums of different diameters and thicknesses of PMMA. Fig. 7(a) shows the diameter of 2500 nm, and Fig. 7(b) the diameter of 3000 cross-section spectrum for thicknesses of 80 nm,85 nm,90 nm, and 100 nm for PMMA.

The dip expands wide for 85 and 90nm thickness and has two higher-order modes. These curves move slightly to the longer wavelength, where the overall curve pattern moves vertically upward. As the diameter of the PMMA disk reaches 3000 nm, we can observe three higher order modes for 80 nm, 95 nm, and 100nm and thickness, while two excited mode peaks are found for 85nm and 90 nm. The dipolar mode completely disappears in curves for the 80 nm, 95 nm, and 100 nm thicknesses. The presence of PMMA due to such diameter does not support any dipolar mode to occur, and only a higher mode exists. In comparison, the dipolar mode expands wide for the 85 and 90 nm thickness; one is very faint higher while another quite significantly higher mode exists. The 85 and 90 nm dip move towards a longer wavelength and the overall curve moves vertically up slightly.

III. Conclusion

By topping a thin layer of photoresist (PMMA) on a gold disc patterned on a silica substrate, we showed that it is feasible to control and vary the fundamental and higher order mode once seen when there was only a gold disk on the glass substrate through the control of topped-up resist thickness and diameter. Furthermore, we have shown that with a diameter of 1500nm, some higher-order modes that arise at various wavelengths, varying thicknesses, and different orders appear to be the same. Additionally, as the PMMA's parameters change, it provides thorough knowledge of the evolution of the PIMI image for each specified wavelength. This method is helpful because it provides an understandable physical explanation for the simulated PIMI pictures of the PMMA-topped metal-dielectric structure. It is very important for understanding controlled modes shapes and their variations generated in PMMA disks on the gold placed on a glass substrate since it has many applications, particularly in sensors and waveguides. To extend the applicability of this approach, it is essential to generalize the numerical implementation of the theory to various particle shapes in a practical manner, which is, in principle, possible and now underway. It has been shown that topping a PMMA resist on a gold disc can change the restricted and higher-order modes created by the gold disc topped on the silica substrate. This can further affect the fundamental and higher-order modes and produce other higher-order mode fields.

Acknowledgments. This work was supported by the National Major Scientific Instruments and Equipment Development Project (No. 61827814), Beijing Natural Science Foundation (No. Z190018), National Natural Science Foundation of China (No. 61627802), Fundamental Research Funds for the Central Universities (No. 30920010011), Ministry of Education collaborative project (B17023), Nanjing University of Science and Technology.

Data availability. All the data are available within the manuscript.

Conflict of Interest. The authors have no any interest.

References

[1]. Yu N., Capasso F., Flat Optics with Designer Meta surfaces, Nat. Mater., 13, 139-150, (2014)
[2]. Minovich A.E., Miroshnichenko A.E., Bykov A.Y., Murzina T.V., Neshev D.N. and Kivshar Y.S., Functional and nonlinear optical metasurfaces, Laser & Photonics Reviews, 9(2), pp.195-213, (2015)
[3]. Li G., Zhang S., Zentgraf T., Nonlinear Photonic Metasurfaces, Nat. Rev. Mater., 2, 17010, (2017)
[4]. Jiang N. Zhuo X., Wang J., Active Plasmonic Principles, Structures, and Applications. Chem. Rev., 118, 3054−3099 (2018)
[5]. Kelly K. L., Coronado E., Zhao L. L., Schatz G. C., The optical properties of metal nanoparticles, The influence of size, shape, and dielectric environment. J. Chem. Phys., 107, 668−677, (2003)
[6]. Krug M. K., Reisecker M., Hohenau A., Ditlbacher H., Trügler A., Hohenester U., Krenn J. R. Probing plasmonic breathing modes optically. Appl. Phys. Lett., 105, 171103 (2014)
[7]. Muravitskaya A., Gokarna A., Movsesyan A., Kostcheev S., Rumyantseva A., Couteau C., Lerondel G., Baudrion A.L., Gaponenko, S.; Adam, P.-M. Refractive index mediated plasmon hybridization in an array of aluminum nanoparticles. Nanoscale, 12, 6394−6402, (2020)

[8]. Movsesyan A., Baudrion A.L., Adam, P.-M. Revealing the Hidden Plasmonic Modes of a Gold Nanocylinder. J. Chem. Phys., 122, 23651−23658, (2018)
[9]. Hao F., Larsson E. M., Ali T. A., Sutherland D. S., Nordlander P. Shedding light on dark plasmons in gold nanoring. Chem. Phys. Lett., 458, 262−266 (2008)
[10]. Chu M.W., Myroshnychenko V., Chen C. H., Deng J., P. Mou C.Y., de Abajo F. J. G., Probing bright and dark surface-plasmon modes in individual and coupled noble metal nanoparticles using an electron beam. Nano Lett., 9, 399−404, (2009)
[11]. Otte M.A., Estevez M.C., Carrascosa L.G., Gonzalez Guerrero A.B., Lechuga L.M., Sepulveda B., Improved biosensing capability with novel suspended nanodisks. J. Chem. Phys., 115, 5344−5351, (2011)
[12]. Muravitskaya A., Gokarna A., Movsesyan A., Kostcheev S., Rumyantseva A., Couteau C., Lerondel G., Baudrion, A.L., Gaponenko S., Adam P.M., Refractive index mediated plasmon hybridization in an array of aluminum nanoparticles, Nanoscale, 12, 6394−6402, (2020)
[13]. Rycenga M., Cobley C. M., Zeng J., Li W., Moran C. H., Zhang Q., Qin D., Xia Y., Controlling the synthesis and assembly of silver nanostructures for plasmonic applications. Chem. Rev., 111, 3669−3712, (2011)
[14]. Lerme J., Bonnet C., Broyer M., Cottancin E., Manchon D., Pellarin M., Optical properties of a particle above a dielectric interface, Cross sections, benchmark calculations, and analysis of the intrinsic substrate effects. J. Chem. Phys., 117, 6383−6398, (2013)
[15]. Knight M.W., Wu,Y.P., Lassiter J.B., Nordlander P., Halas N. J., Nano Lett., 9 (5), 2188–2192, (2009)
[16]. Wu Y. P., Nordlander P. J., Phys. Chem. C, 114 (16), 7302–7307, (2010)
[17]. Vernon K. C., Funston A. M., Novo C., Gomez D. E., Mulvaney P., Davis T. J., Nano Lett., 10 (6), 2080–2086, (2010)
[18]. Sherry L. J., Chang S.H., Schatz G. C., Van Duyne R. P., Wiley B. J., Xia Y., Localized surface plasmon resonance spectroscopy of single silver nanocube, Nano Lett., 5, 2034−2038, (2005)
[19]. Zhang S., Bao .K., Halas N. J., Xu H., Nordlander P., Substrate-induced Fano resonances of a plasmonic nanocube: a route to increased-sensitivity localized surface plasmon resonance sensors revealed. Nano Lett., 11, 1657−1663, (2011)
[20]. Artur M., Alina M., Marion C., Sergei K., Julien P., Jérôme P., Anne L.B., Rémi V., Pierre M.A., Hybridization and Dehybridization of Plasmonic Modes The Journal of Physical Chemistry C, 125 (1), 724-731, (2021)
[21]. The simulations were performed by the FDTD solutions trademark software. http://www.lumerical.com
[22]. Rakic A.D., Djurisic A.B., Elazar J.M., Majewski M.L., Appl opt 37:5271–5283, (1998)
[23]. Palik ED., Handbook of Optical Constants of Solids III (Academic), (1998)
[24]. Liu X., Qiu B., Chen Q., Ni Z., Jiang Y., Long M., Gui L., Characterization of Graphene Layers Using Super Resolution Polarization Parameter Indirect Microscopic Imaging. Opt. Express, 22 (17), 20446, (2014)